# Amphiphilic Triblock Copolymers from Poly(2-oxazoline) with Different Hydrophobic Blocks: Changes of the Micellar Structures upon Addition of a Strongly Hydrophobic Cancer Drug

Sebastian Jaksch, Anita Schulz, Zhenyu Di, Robert Luxenhofer, Rainer Jordan, Christine M. Papadakis*

Dedicated to the late Karl-Friedrich Arndt

Amphiphilic triblock copolymers with poly(2-methyl-2-oxazoline) (MeOx) end blocks and a poly(2-n-butyl-2-oxazoline) (nBuOx) middle block have been found to solubilize large amounts of the cancer drug paclitaxel (PTX) whereas this is not the case when the middle block is more hydrophobic, such as poly(2-n-nonyl-2-oxazoline) (NOx) (Schulz et al., *ACS Nano* 2014, *8*, 2686). To further elucidate the origin of this behavior, dilute aqueous solutions (5–10 mg mL^{-1}) of these two copolymers have been investigated by small-angle neutron scattering (SANS), both in the absence and presence of PTX. Whereas PMeOx-*b*-PNOx-*b*-PMeOx forms mainly worm-like micelles coexisting with large aggregates, spherical micelles are predominant in PMeOx-*b*-PnBuOx-*b*-PMeOx. Already small PTX concentrations lead to shape changes in PMeOx-*b*-PNOx-*b*-PMeOx toward spherical micelles. In contrast, changes in the aggregation behavior of PMeOx-*b*-PnBuOx-*b*-PMeOx are only observed at higher PTX concentrations with a transformation into raspberry-like particles, which may explain the high PTX loading capacity of PMeOx-*b*-PnBuOx-*b*-PMeOx micelles.
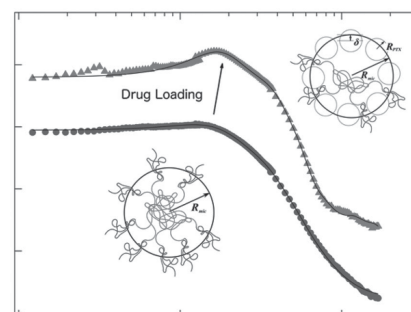
Dr. S. Jaksch,[+] Prof. C. M. Papadakis
Physik-Department
Physik weicher Materie
Technische Universität München
James-Franck-Str. 1, 85748 Garching, Germany
E-mail: papadakis@tum.de
Dr. A. Schulz,[++] Prof. R. Jordan
Department Chemie
Professur für Makromolekulare Chemie
Technische Universität Dresden
Mommsenstr. 4, 01069 Dresden, Germany
Dr. Z. Di
Jülich Centre for Neutron Science JCNS
Forschungszentrum Jülich GmbH
Outstation at MLZ
Lichtenbergstr. 1, 85748 Garching, Germany

Prof. R. Luxenhofer
Functional Polymer Materials
Chair of Chemical Technology of Materials Synthesis
University Würzburg
Röntgenring 11, 97070 Würzburg, Germany

[+]Present address: Jülich Centre for Neutron Science JCNS, Forschungszentrum Jülich GmbH, Outstation at MLZ, Lichtenbergstr. 1, 85748 Garching, Germany
[++]Present address: Institut des Biomolécules Max Mousseron (IBMM), UMR CNRS 5247, University of Montpellier, Faculty of Pharmacy, 15 Av. C. Flahault, Montpellier 34093, France

1. Introduction

Drug formulation is one of the most crucial issues in pharmaceutical technology, especially for poorly water-soluble drugs. For instance, paclitaxel (PTX), a potent cytostatic drug, clinically used for the treatment of a number of tumors, has a water solubility of only 1 µg mL^{-1}.[1–6] For its delivery, several approaches such as nano- and microparticles,[7] liposomes,[5,8] and polymeric micelles[1,3,6,9,10] have been studied with the aim of achieving a high loading capacity and solubility. This, in turn, reduces the administered amount of excipient, limits excipient related toxicities, and enables efficient patient treatment with small volumes of formulation. However, currently used clinical formulations only allow less than 1 wt% (Taxol) or 10 wt% (Abraxane) of active drug, and the carriers may cause considerable side effects.[11,12]

Doubly amphiphilic poly(2-oxazoline)s (POx) were found to be efficient as a drug delivery system for the hydrophobic PTX and structurally similar taxoids[21] with an unprecedented high loading capacity of almost 50 wt%[13] and excellent shelf stability of more than half a year.[14] Since POx is synthesized by means of living cationic ring-opening polymerization (LCROP), the polymers can be tailored with respect to their composition, sequence, architecture, and chemical functionality, and can be well reproduced. In combination with low toxicity and limited complement activation, POx has become an interesting and versatile platform for a variety of biomedical applications over the last decades.[13–21]

Interestingly, although PTX is very hydrophobic, the best solubilization results were achieved with micelles formed by amphiphilic ABA triblock copolymers comprising a *weakly* hydrophobic core of 2-butyl-2-oxazoline (BuOx) and hydrophilic poly(2-methyl-2-oxazoline) (MeOx) end blocks. In contrast, a poly(2-*n*-nonyl-2-oxazoline) (NOx) containing triblock copolymer PMeOx-*b*-PNOx-*b*-PMeOx was much less capable in solubilizing high amounts of PTX and was also significantly less stable over time, as described before.[14] In this study, both amphiphilic block copolymers, PMeOx-*b*-PNOx-*b*-PMeOx and PMeOx-*b*-PBuOx-*b*-PMeOx, were characterized by various scattering and microscopy methods, and it was found that the shape of the micelles formed by PMeOx-*b*-PBuOx-*b*-PMeOx changed from partially worm-like to exclusively spherical upon loading with even small amounts of PTX. The finding of worm-like micelles corroborates previous findings on POx block copolymers with strongly hydrophobic blocks, namely, 2-*n*-nonyl-2-oxazoline and 2-phenyl-2-oxazoline,[22] as well as 2-(2,6-difluorophenyl)-2-oxazoline, 2-(2,4,6-trifluorophenyl)-2-oxazoline,

2-(2,4,5,6-tetrafluorophenyl)-2-oxazoline, and 2-(2,3,4,5,6-pentafluorophenyl)-2-oxazoline,[23] and perfluorinated POx blocks.[24]

To elucidate the structural origin of the divergent behavior of PMeOx-*b*-PNOx-*b*-PMeOx and PMeOx-*b*-P*n*BuOx-*b*-PMeOx and the effect for drug solubilization, we used small-angle neutron scattering (SANS) on aqueous solutions of these polymers with different PTX loading. Recently, we reported briefly on the SANS results for PMeOx-*b*-P*n*BuOx-*b*-PMeOx in conjunction with dynamic light scattering, atomic force microscopy, and (cryogenic) transmission electron microscopy.[14] Only the most important SANS results were given, without going into the details of the data analysis. In the present paper, we present the results of this investigation in detail and, moreover, correlate these with our recent results on PMeOx-*b*-PNOx-*b*-PMeOx in the presence and absence of PTX, as obtained by SANS.

2. Experimental Section

2.1. Materials

All chemicals were purchased from Sigma-Aldrich (Munich, Germany) and Acros Organics (Geel, Belgium). PTX was obtained from LC Laboratories (Woburn, MA). The polymers were synthesized by cationic ring opening polymerization as described in the previous study.[14] Their molar masses and dispersities are compiled in Table 1.

Solutions of the triblock copolymers were prepared by dissolving PMeOx$_{35}$-*b*-PNOx$_{14}$-*b*-PMeOx$_{35}$ and PMeOx$_{33}$-*b*-P*n*BuOx$_{26}$-*b*-PMeOx$_{45}$ in D$_2$O (99.9%, Deutero GmbH, Kastellaun, Germany) at c_{pol} = 10 mg mL^{-1}. The former was annealed for 3 h at 70 °C to obtain a clear solution. Drug-loaded sample solutions were prepared via a thin film hydration method. Stock solutions of polymer and PTX in ethanol were mixed in the desired ratios. The ethanol was removed via a steady hot air flow (≈100 °C, 20 min) and subsequent vacuum. The resulting thin films were rehydrated with deionized water and kept at 55 °C for 5–20 min. Afterward, the aqueous solutions were filtered with a polyvinylidene fluoride (PVDF) filter with a pore size of 0.45 µm, freeze-dried for transport and rehydrated in D$_2$O for measurement.[14] All samples dissolved readily, except the PMeOx$_{35}$-*b*-PNOx$_{14}$-*b*-PMeOx$_{35}$/PTX formulation, which had to be heated to 40 °C for ≈15 min to achieve complete dissolution. The PTX contents were determined via HPLC as described

■ *Table 1.* Polymer characteristics.

	M_n[a] [kg mol^{-1}]	Đ[b]	HLB[c]
PMeOx$_{35}$-*b*-PNOx$_{14}$-*b*-PMeOx$_{35}$	8.8	1.28	14
PMeOx$_{33}$-*b*-P*n*BuOx$_{26}$-*b*-PMeOx$_{45}$	10.0	1.14	13

[a]Molar masses M_n determined by ^{1}H NMR; [b]Dispersities Đ determined by GPC; [c]Hydrophilic–lipophilic balance HLB = 20×[1-($M_{hydrophobic block}$/$M_{polymer}$)].

Materials
Views
www.MaterialsViews.com

Macromol. Chem. Phys. **2016**, *217*, 1448–1456
© 2016 WILEY-VCH Verlag GmbH & Co. KGaA, Weinheim

Macromolecular
Journals

1449

■ *Table 2.* Polymer and PTX concentrations of the solutions used for SANS.

Polymer	c_{Pol} [mg mL^{-1}]	c_{PTX} [mg mL^{-1}]	LC[a]
PMeOx$_{35}$-b-PNOx$_{14}$-b-PMeOx$_{35}$	5.0	0	n/a
	5.0	0.17	3.3
PMeOx$_{33}$-b-PnBuOx$_{26}$-b-PMeOx$_{45}$	9.9	0	n/a
	9.0	0.2	2.2
	10.0	0.9	8.3
	9.9	1.9	16.1
	8.6	4.2	32.8
	10.0	4.8	32.4

[a] $m_{PTX}/m_{total} \times 100\%$.

previously[14] and are listed together with the corresponding loading capacities (LC) in Table 2.

2.2. Small-Angle Neutron Scattering (SANS)

SANS experiments were performed at the KWS-1 instrument at the JCNS outstation at Heinz Maier-Leibnitz Zentrum, MLZ, in Garching. In most experiments, a neutron wavelength $\lambda = 6.9$ Å ($\Delta\lambda/\lambda = 10\%$) and sample-detector distances (SDD) of 1.72 m, 7.72 m, and, in some cases, 19.72 m were used to expand the q range ($q = 4\pi\sin(\theta/2)/\lambda$ is the momentum transfer with θ the scattering angle). The curve of PMeOx$_{35}$-b-PNOx$_{14}$-b-PMeOx$_{35}$ loaded with PTX was measured at $\lambda = 4.9$ Å ($\Delta\lambda/\lambda = 10\%$) and at SDDs of 1.72 and 7.72 m. In all experiments, the detector was a ^{6}Li glass scintillation detector with an active area of 60 cm × 60 cm. Exposure times were 5 min at SDD = 1.72 m, 15 min at SDD = 7.72 m and 30 min at SDD = 19.72 m. The samples were mounted in flat Hellma quartz-glass cuvettes with a light path of 2 mm. These were placed in an aluminum oven, which was temperature-controlled by a Julabo thermostat. The experiments were conducted at 37 °C. Dark current correction was carried out using boron carbide. The scattering of D$_2$O and the empty cell were subtracted from the sample scattering, taking the transmissions into account. Poly(methyl methacrylate) was used to bring the data to absolute scale and to determine the detector sensitivity. The resulting intensities were azimuthally averaged. Good agreement was found in the overlap regions of the curves measured at different SDDs. All data reduction steps were performed with the software QtiKWS provided by JCNS.

2.3. Modeling of SANS Curves

For fitting the SANS curves, the following expression was used:

$$I(q) = P(q)S_{HS}(q) + I_{agg}(q) + I_{bkg} \tag{1}$$

$P(q)$ is the form factor describing the shape and structure of the micelles, $S_{HS}(q)$ is the structure factor describing their correlation, $I_{agg}(q)$ is the forward scattering from large aggregates, and I_{bkg} is the incoherent background. The respective expressions are given below.

2.3.1. PMeOx$_{35}$-b-PNOx$_{14}$-b-PMeOx$_{35}$

For the unloaded and loaded PMeOx$_{35}$-b-PNOx$_{14}$-b-PMeOx$_{35}$ solutions, no structure factor was needed, and $S_{HS}(q)$ was therefore set to one. For the unloaded solutions, a form factor for worm-like micelles proved to be suitable for $P(q)$[25,26]

$$P_{worm}(q) = w(q, R_g)\frac{2(\exp(-qR_g) + qR_g - 1)}{q^2 R_g^2}$$
$$+ (1 - w(q, R_g))\left[C_1(qR_g)^{-1/0.585}\right. \tag{2}$$
$$\left. + C_2(qR_g)^{-2/0.585} + C_3(qR_g)^{-3/0.585}\right]$$

where

$$w(x) = \left[1 + \tanh\left((x - C_4)/C_5\right)\right]/2 \tag{3}$$

is an empirical function and $C_1 = 1.220$; $C_2 = 0.4288$; $C_3 = -1.651$; $C_4 = 1.523$, and $C_5 = 0.1477$ are numerical constants.[23] The radius of gyration, R_g, of the worm-like micelles reads

$$\langle R_g^2\rangle = \alpha\left(\frac{L}{b}\right)^2\langle R_g^2\rangle_o \tag{4}$$

Here, $\langle R_g^2\rangle_o$ denotes the radius of gyration in the case of vanishing excluded volume interaction. L and b are the contour length and the persistence length of the worm-like micelles and are free parameters during the fit. The factor $\alpha(x)$ is an empirical function given by

$$\alpha(x)^2 = \left[1 + \left(\frac{x}{3.12}\right)^2 + \left(\frac{x}{8.67}\right)^3\right]^{0.170/3} \tag{5}$$

The polydispersity of the cross section radius is taken into account by convolution of $P_{worm}(q)$ with a Schulz–Zimm distribution function. The cross-section radius R is found by a Guinier fit[27] in the intermediate q-regime.[26] The form factor was normalized with the volume fraction of the worm-like micelles.

The forward scattering due to large aggregates was fitted by a power law[28]

$$I_{agg}(q) = I_{PL}^o \times q^{-\alpha} \tag{6}$$

with I_{PL}^o being the prefactor and α an exponent related to the surface structure of the aggregates.

For the PTX loaded solutions of PMeOx$_{35}$-b-PNOx$_{14}$-b-PMeOx$_{35}$, the micelles were not worm-like, and a form factor for polydisperse homogeneous spheres was more suitable[29]

$$P_S(q) = N_S V_S^2(\rho_{pol} - \rho_{D_2O})^2\left(\frac{3(\sin(qR_{mic}) - qR\cos(qR_{mic}))}{(qR_{mic})^3}\right)^2 \tag{7}$$

N_S is the number of spheres, V_S is the sphere volume, ρ_{pol} and ρ_{D2O} are the scattering length densities of the polymer and D$_2$O, respectively, and R_{mic} the average sphere radius. To account for polydispersity, a Schulz–Zimm distribution of R_{mic} was included.[30]

1450

Macromolecular
Journals

Macromol. Chem. Phys. **2016**, *217*, 1448–1456
© 2016 WILEY-VCH Verlag GmbH & Co. KGaA, Weinheim

Materials
Views

www.MaterialsViews.com

Amphiphilic Triblock Copolymers from Poly(2-oxazoline) with Different Hydrophobic Blocks . . .

Macromolecular
Chemistry and Physics
www.mcp-journal.de

2.3.2. PMeOx$_{33}$-b-PnBuOx$_{26}$-b-PMeOx$_{45}$

For the solutions of unloaded and loaded PMeOx$_{33}$-b-PnBuOx$_{26}$-b-PMeOx$_{45}$, the aggregate scattering $I_{agg}(q)$ in Equation (1) was set to zero. As a structure factor, the Percus–Yevick structure factor for hard spheres was used, i.e., the correlation between the micelles is liquid-like[31]

$$S_{HS}(q) = \frac{1}{1 + 24\eta_{HS}G(2\eta R_{HS}q)/(2\eta R_{HS}q)} \tag{8}$$

R_{HS} is the hard-sphere radius which, in our case, is equivalent to half the distance between the centers of two micelles. The volume fraction of the correlated particles, η_{HS}, is the volume occupied by the hard spheres in comparison to the total volume. The function $G(x)$ is defined by

$$G(x) = \gamma \frac{\sin x - x\cos x}{x^2} + \delta \frac{2x\sin x + (2 - x^2)\cos x - 2}{x^3}$$
$$+ \varepsilon \frac{-x^4\cos x + 4(3x^2 - 6\cos x + (x^3 - 6x)\sin x + 6)}{x^5} \tag{9}$$

where the help functions are given by

$$\gamma = \frac{(1 + 2\eta_{HS})^2}{(1 - \eta_{HS})^4}; \delta = \frac{-6\eta_{HS}(1 + \eta_{HS}/2)^2}{(1 - \eta_{HS})^4}; \varepsilon = \frac{\gamma\eta_{HS}}{2} \tag{10}$$

The form factor of the drug loaded micelles was found to depend strongly on PTX concentration. At low PTX concentrations (0 and 0.2 mg mL^{-1}), the form factor for polydisperse, homogeneous spheres, $P_S(q)$ (Equation (7)) was used. At higher PTX concentrations, the sphere form factor did not describe the curves adequately; instead, the curves were modeled with a form factor for raspberry-like micelles (Figure 1).[32] This model assumes small spherical particles (in the present case PTX domains) indented by a depth δ into the surface of larger spherical particles. The relevant parameters obtained from the
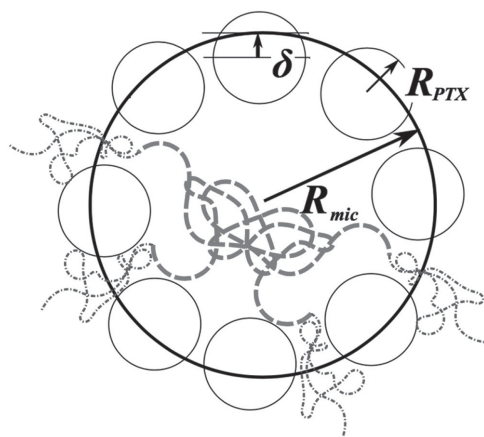

Figure 1. Sketch of the structure of the raspberry-like micelle. R_{mic} and R_{PTX} are the radii of the polymer micelle and the embedded PTX domains, respectively. The immersion depth of these domains, measured from the surface of the complex, is given by δ. The assumed location of the hydrophobic core blocks of PMeOx$_{33}$-b-PnBuOx$_{14}$-b-PMeOx$_{45}$ is drawn in red (dashed bold line), the hydrophilic blocks forming the shell in blue (dashed-dotted thinner line). The shell blocks are assumed to protrude between the PTX particles.

fits are the radii of the small particles and the micelles, R_{PTX} and R_{mic}, the indentation depth δ, the surface coverage and the polydispersity of R_{mic}.

In all fits, the scattering-length densities of D$_2$O and of the POx polymers were kept constant at $\rho_{D2O} = 6.36 \times 10^{-6}$ Å^{-2} and $\rho_{POx} = 0.2 \times 10^{-6}$ Å^{-2}, respectively. The first value is the literature value. The latter was found consistently from fitting the SANS curves and is within the expected range of $(0.2–0.8) \times 10^{-6}$ Å^{-2} for the core-forming blocks PNOx and PnBuOx. It is consistent with the mass density of 1.05 g cm^{-3},[33] and the values reported by Ivanova et al.,[22] albeit at the lower limit. The scattering length density of PTX was used as a free parameter during the fit. The resulting values $\rho_{PTX} = 2 \times 10^{-6}$ Å^{-2} to 4×10^{-6} Å^{-2} are in agreement with the theoretical value of $\rho_{PTX} = 2.1 \times 10^{-6}$ Å^{-2} (calculated from the molecular composition of PTX and its mass density of 1.4 g cm^{-3}).[34] The incoherent background was fitted in preliminary fits and was in all cases found at 0.005–0.05 cm^{-1}. To reduce the amount of free parameters, the incoherent background was set to 0.02 cm^{-1} for the PMeOx$_{33}$-b-PnBuOx$_{26}$-b-PMeOx$_{45}$ data. For the curves from PMeOx$_{35}$-b-PNOx$_{14}$-b-PMeOx$_{35}$ solutions, it was left free and resulted in 0.08 and 0.056 cm^{-1} without and with PTX, respectively. All fitting procedures described above were carried out using the NIST NCNR SANS package for IGOR Pro[35] and procedures written by the authors. The most important parameters are given in the text below; the full parameter sets are given in the Supporting Information (Tables S1–S4).

3. Results and Discussion

In this section, we present detailed information on the shape and inner structure of the micelles from the two systems PMeOx$_{35}$-b-PNOx$_{14}$-b-PMeOx$_{35}$ and PMeOx$_{33}$-b-PnBuOx$_{26}$-b-PMeOx$_{45}$ obtained using SANS, both for the unloaded and the PTX loaded micellar solutions. These two polymers were chosen due to their overall similar hydrophilic/lipophilic balance, while having a large difference in the hydrophobicity of the micellar core (Table 1). The polymer concentration was chosen at $c_{pol} \cong 5–10$ mg mL^{-1} and the temperature at 37 °C, i.e., close to physiological conditions. Using D$_2$O as a solvent ensures maximum scattering contrast between the (drug-loaded) micelles and the solvent.

3.1. PMeOx$_{35}$-b-PNOx$_{14}$-b-PMeOx$_{35}$

The SANS curves of the polymer at a concentration of 5.0 mg mL^{-1} in the unloaded state as well as loaded with 0.17 mg mL^{-1} PTX are shown in Figure 2a. At intermediate q values (0.003 Å$^{-1} < q < 0.03$ Å^{-1}), the SANS curve from the pure polymer solution (see also Figure 2b) features a decay following approximately $I(q) \propto q^{-\alpha}$ with $\alpha = 1–2$. A value $\alpha = 1$ is indicative of a rod-like shape of the micelles, whereas worm-like micelles (Gaussian conformation) give rise to $\alpha = 2$. The decay at $q < 0.003$ Å^{-1} is slightly steeper;
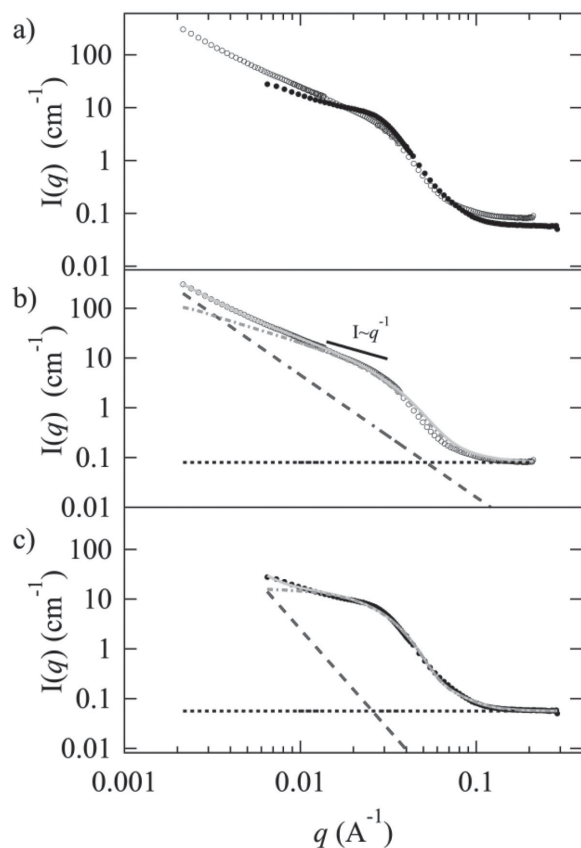
a)

Figure 2. a) SANS curves of a 5 mg mL^{-1} solution of PMeOx$_{35}$-*b*-PNOx$_{14}$-*b*-PMeOx$_{45}$ without PTX (open symbols) and with 0.17 mg mL^{-1} PTX (closed symbols). Same curves b) without PTX and c) with 0.17 mg mL^{-1} PTX. The full orange lines are the full fitting functions, the green dashed-dotted lines the form factor of the micelles, $P(q)$, the blue dashed lines are the form factor of large aggregates, $I_{agg}(q)$ (Equation (6)), and the black dashed lines are the incoherent background, I_{bkg}. For the unloaded micelles (b), the form factor of worm-like micelles (Equations (2)–(5)) was used for $P(q)$, whereas for the loaded micelles (c), the form factor of polydisperse spheres (Equation (7)) was used. The short full line in (b) indicates the behavior $I(q) \propto q^{-1}$.

thus, larger aggregates are present as well. At high q values ($q > 0.03$ Å^{-1}), a very steep decay is present, reflecting the cross-section scattering of the worm-like micelles. The curve from PTX-loaded polymer (see also Figure 2c) differs significantly, especially the decay at 0.03–0.1 Å^{-1}. This indicates that the morphology of the micelles depends on the loading with PTX, as previously observed.[14]

The model used for fitting the SANS data of the pure PMeOx$_{35}$-*b*-PNOx$_{14}$-*b*-PMeOx$_{35}$ triblock copolymer (Figure 2b, Equations (1)–(6)) includes the scattering from uncorrelated, homogeneous worm-like particles of circular cross-section together with scattering from large aggregates. The fit (full orange line in Figure 2b) is very good over the entire q range, and only a slight deviation is observed in the region of the steep decay. Possible reasons for this deviation are discussed below. From the fit,

the contour length and persistence length of the worm-like micelles are $L = 2030 \pm 500$ Å and $b = 1360 \pm 70$ Å (Figure 3). Since L is only a factor of 1.5 larger than b, the micelles are relatively stiff. The micellar cross-section radius is 41 ± 7 Å with a polydispersity of 0.3. The latter value may be overestimated because the resolution function was not taken into account. To account for the slightly steeper decay of the scattering at low q values, a weak contribution proportional to $q^{-2.5\pm0.1}$ was used as $I_{agg}(q)$, i.e., large aggregates are present as well. Interestingly, neither for this nor for the other samples, a core–shell structure could be detected, which may be due to the missing scattering contrast between the loosely packed shell (which is well hydrated) and the solvent environment. The cross-section radius thus rather refers to the core radius, possibly also with contributions of the inner part of the shell which is more densely packed.

The rod-like shape of the micelles corroborates the results found by us previously using transmission electron microscopy (TEM) on stained samples.[14] These experiments revealed homogeneous spherical micelles with radii of 46 ± 12 Å with few worm-like structures having cross-section radii of 48.6 ± 2.1 Å and lengths of 340–1520 Å, which is smaller but still consistent with the value of L found by SANS (see above). The presence of spherical micelles in the solution may be the origin of the deviation of the fitting curve from the SANS data. We have attempted to fit a model including both the described cylinders and homogeneous spheres; however, the fraction of the latter is very small, and the fit was unstable. A core–shell structure of the micelles has not been included in the fitting function. In our previous SANS study on a PNOx$_{10}$-*b*-PMeOx$_{32}$ diblock copolymer in D$_2$O, a core–shell structure was not evident either, and only in carefully chosen mixtures of D$_2$O and H$_2$O matching the scattering length densities of PMeOx and PNOx, the core–shell structure could be obtained in a combinatorial approach.[24]

For the SANS curve of the PMeOx$_{35}$-*b*-PNOx$_{14}$-*b*-PMeOx$_{35}$ in D$_2$O loaded with 0.17 mg mL^{-1} of PTX (Figure 2c), the best fit was achieved using the form factor of polydisperse, homogeneous spheres (Equations (1) and (7)). Fits
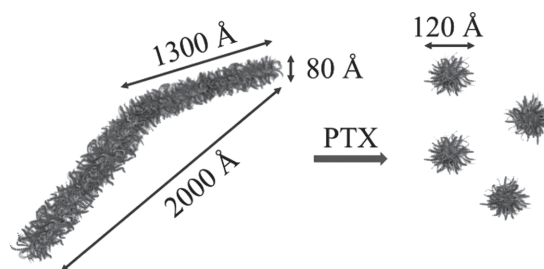

Figure 3. Graphical representation of the morphological transition from worm-like to spherical PMeOx$_{35}$-*b*-PNOx$_{14}$-*b*-PMeOx$_{35}$ micelles upon loading with PTX. Diameters and lengths are indicated.

www.MaterialsViews.com

Amphiphilic Triblock Copolymers from Poly(2-oxazoline) with Different Hydrophobic Blocks . . .

Macromolecular
Chemistry and Physics
www.mcp-journal.de

using the worm-like micelle model were not successful. The sphere radius is 59.81 ± 0.03 Å with a polydispersity of 0.25. Again, a power law for the forward scattering was included, and an exponent $\alpha = -4.01 \pm 0.03$ was found, as expected for compact aggregates with a smooth surface. However, since the measured q range in this case is limited towards low values, only few data points contribute to this term.

These results are consistent with our previous observations using atomic force microscopy (AFM).[14] For a PTX content of 0.2 mg mL^{-1}, distorted uniform spheres of roughly 50 Å in height and 400–500 Å in diameter were observed. The distortion of the micelles was attributed to their flattening upon contact with the surface, which may result in overestimation of their radii. Here, we provide evidence that, in solution, the PTX loaded micelles are spherical, which corroborates our previous results that, in aqueous solution of PMeOx-b-PNOx-b-PMeOx triblock copolymers, incorporation of PTX leads to a change of shape of the micelles from worm-like to spherical (Figure 3).

3.2. PMeOx$_{33}$-b-PnBuOx$_{26}$-b-PMeOx$_{45}$

To investigate the structures of the micelles formed by the weakly amphiphilic triblock copolymer and to better

understand the origin of the high drug loading capacity, SANS was carried out on solutions of pure PMeOx$_{33}$-b-Pn-BuOx$_{26}$-b-PMeOx$_{45}$ in D$_2$O and on solutions loaded with PTX at several concentrations $c_{PTX} = 0.2$–4.8 mg mL^{-1}. For all solutions, the polymer concentration was chosen at $c_{pol} \cong 10$ mg mL^{-1}. The drug-loaded systems were prepared following the same protocol as described previously[14] with an additional intermediate freeze-drying step for the transport. The scattering curves shown in Figure 4a reveal significant changes of the curve shape upon loading with PTX. For the unloaded solutions and for $c_{PTX} = 0.2$ mg mL^{-1}, a plateau at low q values, a shallow maximum at $q = 0.015$ Å^{-1} and a smooth decay at higher q values is observed. At $c_{PTX} = 0.9$ mg mL^{-1} (8.3 wt%), the maximum becomes more pronounced and moves to higher q values. At higher concentrations (1.9–4.8 mg mL^{-1}), the maximum becomes even more pronounced, changes shape and moves to lower q values with increasing c_{PTX}. This maximum indicates the correlation between the micelles. Moreover, a secondary maximum arises at $q = 0.1$ Å^{-1}. For all values of c_{PTX}, the shape of the curves differs significantly from the ones of the unloaded and loaded solutions of PMeOx$_{35}$-b-PNOx$_{14}$-b-PMeOx$_{35}$ solution (Figure 2a). The decay at low q values, indicative of rod-like particles, is not present in the curves but the intensity is rather constant
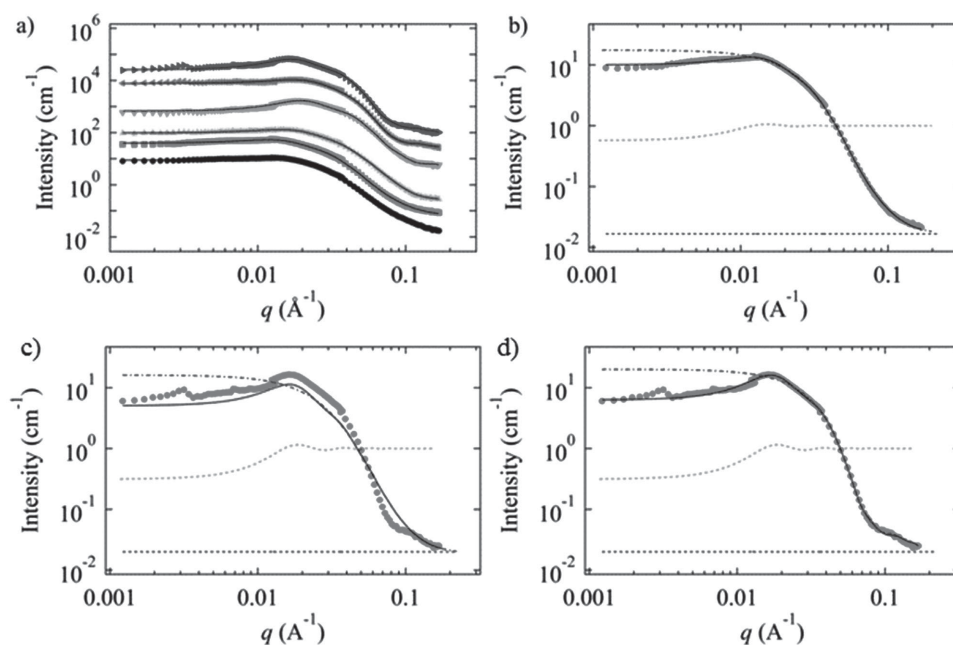

Figure 4. a) SANS curves of PMeOx$_{33}$-b-PnBuOx$_{26}$-b-PMeOx$_{45}$ solutions ($c_{pol} \cong 10$ mg mL^{-1}) in D$_2$O at 37 °C with PTX concentrations of (from below): 0, 0.2 mg mL^{-1}, 0.9 mg mL^{-1}, 1.9 mg mL^{-1}, 4.2 mg mL^{-1}, and 4.8 mg mL^{-1}. The curves were shifted vertically by factors of 4, 16, 256, 1024, and 4096 for better visibility. The full lines are fits of Equation (1). The form factor for homogeneous spheres was used for $c_{PTX} = 0$ and 0.2 mg mL^{-1} and the raspberry form factor for $c_{PTX} = 0.9$–4.8 mg mL^{-1}. b) Example of a fit of the homogeneous sphere model to the SANS data from 0.2 mg mL^{-1} PTX. Fit using c) the homogeneous sphere model and using d) the raspberry form factor to the SANS data of 4.8 mg mL^{-1} PTX. In (a–d), the symbols denote the experimental data and the solid black lines denote the total fitting function. In (b–d), the components of the fitting function are shown as well: The green dashed line is the Percus–Yevick hard-sphere structure factor (Equations (8)–(10)) and the black dashed line is the incoherent background. The blue dashed-dotted line is the respective form factor (homogeneous sphere in (b) and (c), raspberry form factor in (d)).

Makrials Views
www.MaterialsViews.com

Macromol. Chem. Phys. **2016**, *217*, 1448–1456
© 2016 WILEY-VCH Verlag GmbH & Co. KGaA, Weinheim

Macromolecular
Journals

1453

over nearly one decade in q, confirming the spherical shape of the drug loaded micelles from PMeOx$_{33}$-b-PnBuOx$_{26}$-b-PMeOx$_{45}$ and the absence of large aggregates.

For model fitting of the curves at low PTX concentration (0 and 0.2 mg mL^{-1}), the micelles were described by a form factor for homogeneous spheres (Equation (7)) and their correlation with a Percus–Yevick structure factor (Equations (8)–(10), Figure 4b). This way, the simplest possible model was used, keeping the number of fitting parameters at a minimum. Excellent fits were obtained over the full q range for both solutions. The parameters resulting from fitting are compiled in Figure 5. The micellar radius is R_{mic} = 45.6 ± 0.1 Å for the pure triblock copolymer and 49.9 ± 0.1 Å at c_{PTX} = 0.2 mg mL^{-1} (Figure 5a) with polydispersities of 0.4 in both cases. The hard-sphere radius, i.e., half the center-to-center distance, is R_{HS} = 167.5 ± 0.2 Å and 190.0 ± 0.2 Å for c_{PTX} = 0 and 0.2 mg mL^{-1} (Figure 5c), and the volume fraction η_{HS} is 0.068 ± 0.0002 and 0.071 ± 0.0002, i.e., very low (Figure 5d). We note, however, that the sample structures may be sensitive to small differences in the sample history.

At higher PTX concentrations, the secondary maximum cannot be captured by the form factor of a homogeneous sphere. Figure 4c shows the SANS curve for c_{PTX} = 4.8 mg mL^{-1} along with the form factor of a homogeneous sphere of R_{mic} = 62 Å and a polydispersity of 0.2, the Percus–Yevick structure factor with R_{HS} = 161 Å and η_{HS} = 0.15 as well as the total fitting function. This model can neither capture the steep decay at 0.02–0.07 Å^{-1} nor the secondary maximum at 0.1 Å^{-1}. The reason is that the form factor of the homogeneous sphere is not sufficiently steep, and since the structure factor in this region is nearly flat, their product is very similar to the pure form factor. We have therefore tried a different approach to the form factor, namely the raspberry model (Figure 1).[30] Other models which were tested during the data evaluation process included core–shell models of spheres and ellipsoids of rotation, both prolate and oblate. However, none of these could describe the data for PTX concentrations between 0.9 and 4.8 mg mL^{-1} as successfully as the raspberry model. The raspberry particles are homogeneous spheres with small spherical particles—which we attribute to PTX domains—immersed at a certain average depth from the surface. As an example, the form factor of this model is shown for c_{PTX} = 4.8 mg mL^{-1} in Figure 4d with the parameters R_{mic} = 54 Å, R_{PTX} = 16.8 Å, δ = −2.7 Å and the relative polydispersity 0.34. It recovers very well the shape of the experimental curve at q > 0.05 Å^{-1}. Combining this raspberry form factor again with the Percus–Yevick hard-sphere structure factor with R_{HS} = 161 Å and η_{HS} = 0.15 and an incoherent background results in a model function which describes the curve very well in the entire q range (Figure 4d). Therefore, the model was used for c_{PTX} = 0.9–4.8 mg mL^{-1}.

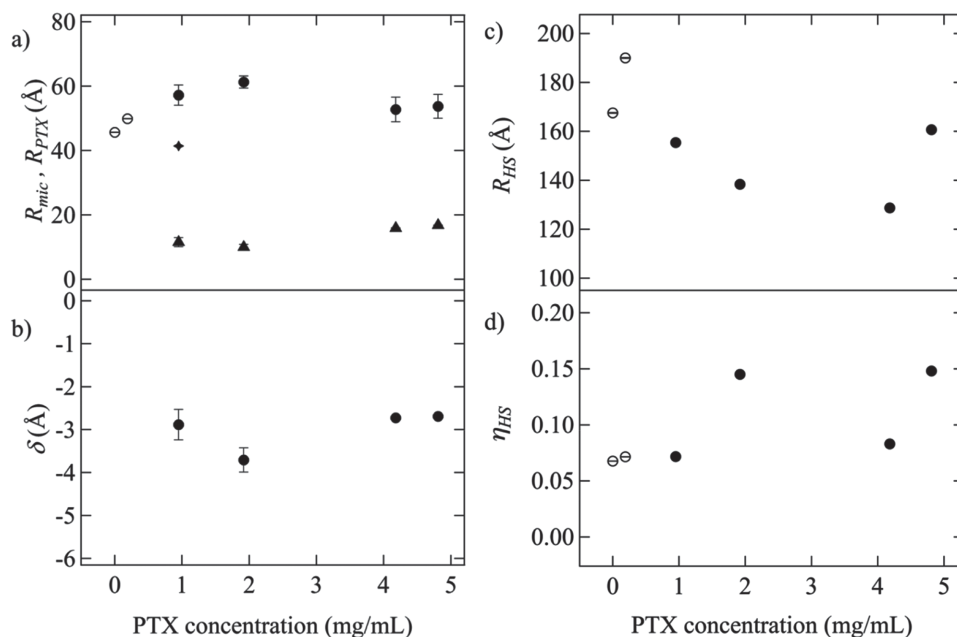To check for consistency, we fitted both models—the homogeneous sphere and the raspberry model—to

Figure 5. Results from model fitting to the SANS curves of PMeOx$_{33}$-b-PnBuOx$_{26}$-b-PMeOx$_{45}$ shown in Figure 4 as a function of the PTX concentration. a) Radii of the spherical micelles (○), of the raspberry complexes (both termed R_{mic}) (●) and of the embedded PTX domains (▲). (♦) R_{mic} from the fit of a simple sphere, see text. b) Immersion depth of the PTX domains, δ. c) Hard-sphere radius, R_{HS}, and d) volume fraction of hard spheres, η_{HS}. Open symbols in (c,d): from the form factor of polydisperse homogeneous spheres, solid symbols: from the raspberry form factor. In some cases, the error bars are smaller than the symbol size.

1454

Macromolecular
Journals

Macromol. Chem. Phys. **2016,** *217,* 1448–1456
© 2016 WILEY-VCH Verlag GmbH & Co. KGaA, Weinheim

www.MaterialsViews.com

Amphiphilic Triblock Copolymers from Poly(2-oxazoline) with Different Hydrophobic Blocks . . .

Macromolecular
Chemistry and Physics

www.mcp-journal.de

the curve of the solution with $c_{PTX} = 0.9$ mg mL^{-1}. The obtained radii of the homogeneous sphere ($R_{mic} = 41.4$ Å) and the raspberry micelle ($R_{mic} = 57.2$ Å) deviate slightly from each other with the raspberry micelle radius being larger (Figure 5a). This is expected, because for a good fit, the fitting function needs to reproduce the first minimum of the form factor. The negative indentation depth shifts the first form factor minimum to higher q-values; thus, the overall size of the raspberry micelle needs to increase for a good fit. This results in an adaptation of the slope in the q-region between $q = 0.02$ and 0.08 Å^{-1} (Figure 5c,d). The hard-sphere radii R_{HS} coincide ($R_{HS} = 154$ Å for the homogeneous spheres and $R_{HS} = 155$ Å for the raspberry micelle) and so does the polydispersity (0.38 and 0.40, respectively). This analysis shows that the models are consistent with each other.

The results from the fits using the raspberry form factor are presented in Figure 5. The radii of the raspberry micelles, R_{mic}, are in the range 53–61 Å (Figure 5a) with polydispersity values between 0.2 and 0.4. Both parameters are independent of c_{PTX}. The radius of the embedded PTX domains increases with c_{PTX} from $R_{PTX} = 11.5 \pm 1.4$ Å at 0.9 mg mL^{-1} to $R_{PTX} = 16.8 \pm 0.1$ Å for 4.8 mg mL^{-1}. Thus, the domains seem to consist of an increasing number of PTX molecules, as their concentration is increased.

The average immersion depth, δ, scatters between -2.7 and -3.7 Å for $c_{PTX} = 0.9$ and 1.9 mg mL^{-1} and $\delta = -2.7 \pm 0.4$ Å for higher c_{PTX} values. The negative sign means that the PTX domains are partially immersed into the particle. We should note that the model considers only one layer of small domains (Figure 1) and not a distribution of immersion depths, which may be more realistic. The δ values from this model may be considered as average values.

The hard-sphere radii lie between $R_{HS} = 128.7 \pm 0.1$ Å and 160.7 ± 0.1 Å, and the volume fraction of hard spheres, η_{HS}, between 0.07 and 0.15, both being independent of c_{PTX}. From the large difference between R_{HS} and R_{mic} (a factor of more than 2) and from the absence of forward scattering in the SANS curves (Figure 4a), we conclude that the micelles from PMeOx$_{33}$-b-PnBuOx$_{26}$-b-PMeOx$_{45}$ do not form large aggregates. This is consistent with previously reported data from electron microscopy.[14]

Since the PMeOx shell of the micelles is presumably loosely packed, and the scattering contrast between the solvent-swollen shell and the solvent is weak, we assume that PTX, at high loading, is located rather in the inner part of the shell close to the micellar PnBuOx core. Possibly, PTX is located at the core–shell interface which we expect to be diffuse and which therefore provides a favorable environment for a complex molecule as PTX (Figure 6). From the diffusion coefficient of PTX, which was previously estimated to be 9.5×10^{-11} m^2 s^{-1},[36] we calculate the hydrodynamic radius of PTX of approximately 26 Å (via the Stokes-Einstein law, using the viscosity of water). Thus, even at high loading, the PTX domains seem to consist of very few PTX molecules, which may associate with the POx triblock copolymers via nonpolar as well as polar interactions. At low PTX loading, we hypothesize, that the PTX is completely immersed in the core, still allowing a homogeneous sphere fit. By increasing the PTX concentration, the molecules are slowly pushed outside the micellar core, resulting in the raspberry shape (Figure 6). We note at this point that the surface coverage of the micelle with PTX (Table S4 in the Supporting Information) is included in the model as a fitting parameter; however, the uncertainties are large, and the parameter rather describes the surface coverage of the core and not the micellar surface. Therefore, we are unable to deduce a correlation between the surface coverage of the PTX domains and the PTX load.

4. Conclusions

We have investigated aqueous solutions of the triblock copolymers PMeOx-b-PNOx-b-PMeOx and PMeOx-b-Pn-BuOx-b-PMeOx which both feature hydrophilic end blocks, whereas the middle blocks are strongly (NOx) or weakly (nBuOx) hydrophobic. Using SANS, detailed information on the micellar size, shape, inner structure, and correlation as well as the changes upon incorporation of the cancer drug paclitaxel (PTX) was obtained in dependence on PTX concentration, which complements our previous TEM investigations.[14] We note that the SANS measurements are carried out in solution, with no preparation steps such as drying, freezing and staining which are needed to do TEM
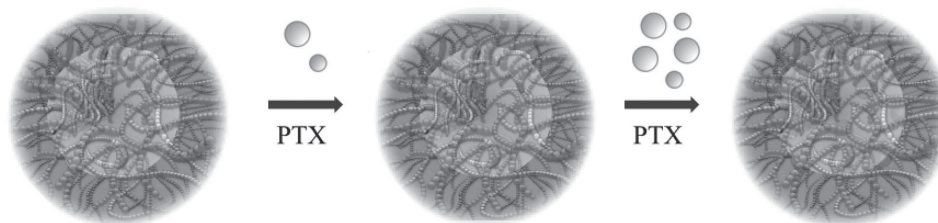

Figure 6. Graphical representation of the loading of PMeOx$_{33}$-b-PnBuOx$_{26}$-b-PMeOx$_{45}$ micelles with PTX. At first, the core is filled with a few PTX particles. If the core is saturated, bumps appear on the surface of the micellar core upon further increase of the PTX loading.

Materials Views
www.MaterialsViews.com

Macromol. Chem. Phys. **2016,** *217,* 1448–1456
© 2016 WILEY-VCH Verlag GmbH & Co. KGaA, Weinheim

Macromolecular
Journals

1455

and which may alter the sample structure. Moreover, SANS averages over a large sample volume, in contrast to TEM, and the results are thus statistically relevant.

The SANS measurements revealed that PMeOx$_{35}$-b-PNOx$_{14}$-b-PMeOx$_{35}$ in D$_2$O forms mainly worm-like micelles which transform into spherical ones upon loading with a small amount of PTX (0.17 mg mL^{-1}). The structures found in this investigation (worm-like micelles) compare well to the ones reported by Fustin et al.[22] The shape changes of the worm-like micelles formed by PMeOx$_{35}$-b-PNOx$_{14}$-b-PMeOx$_{35}$ triblock copolymers to spherical ones upon addition of PTX hint to a PTX/core interaction which is similar to PMeOx$_{33}$-b-PnBuOx$_{26}$-b-PMeOx$_{45}$, as we have discussed previously.[14]

The formation of the raspberry-like structure of PMeOx$_{33}$-b-PnBuOx$_{26}$-b-PMeOx$_{45}$ micelles may explain its much better loading capacity as compared to PMeOx$_{35}$-b-PNOx$_{14}$-b-PMeOx$_{35}$ micelles despite their comparable size. Not only is PTX immersed in the core, but also decorates the core/shell interface. The incorporation of PTX beyond the confinements of the hydrophobic core may be one of the reasons for the tremendous loading capacity of the described POx based polymer when compared to other POx amphiphiles and conventional excipients, respectively.[37]

Supporting Information

[1] R. Savic, L. B. Luo, A. Eisenberg, D. Maysinger, *Science* **2003**, *300*, 615.

[2] R. Haag, *Angew. Chem. Int. Ed.* **2004**, *43*, 278.

[3] V. P. Torchilin, *Cell. Mol. Life Sci.* **2004**, *61*, 2549.

[4] R. D. Dabholkar, R. M. Sawant, D. A. Mongayt, P. V. Devarajan, V. P. Torchilin, *Int. J. Pharm.* **2006**, *315*, 148.

[5] T. Yang, F. D. Cui, M. K. Choi, J. W. Cho, S. J. Chung, C. K. Shim, D. D. Kim, *Int. J. Pharm.* **2007**, *338*, 317.

[6] A. V. Kabanov, S. V. Vinogradov, *Angew. Chem. Int. Ed.* **2009**, *48*, 5418.

[7] N. P. Desai, V. Trieu, L. Y. Hwang, R. J. Wu, P. Soon-Shiong, W. J. Gradishar, *Anti-Cancer Drugs* **2008**, *19*, 899.

[8] J. Wu, Q. Liu, R. J. Lee, *Int. J. Pharm.* **2006**, *316*, 148.

[9] K. Kataoka, A. Harada, Y. Nagasaki, *Adv. Drug Delivery Rev.* **2001**, *47*, 113.

[10] Y. Matsumura, K. Kataoka, *Cancer Sci.* **2009**, *100*, 572.

[11] H. Gelderblom, J. Verweij, K. Nooter, A. Sparreboom, *Eur. J. Cancer* **2001**, *37*, 1590.

[12] K. L. Hennenfent, R. Govindan, *Ann. Oncol.* **2006**, *17*, 735.

[13] R. Luxenhofer, A. Schulz, C. Roques, S. Li, T. K. Bronich, E. V. Batrakova, R. Jordan, A. V. Kabanov, *Biomaterials* **2010**, *31*, 4972.

[14] A. Schulz, S. Jaksch, R. Schubel, E. Wegener, Z. Di, Y. Han, A. Meister, J. Kressler, A. V. Kabanov, R. Luxenhofer, C. M. Papadakis, R. Jordan, *ACS Nano* **2014**, *8*, 2686.

[15] T. X. Viegas, M. D. Bentley, J. M. Harris, Z. F. Fang, K. Yoon, B. Dizman, R. Weimer, A. Mero, G. Pasut, F. M. Veronese, *Bioconjugate Chem.* **2011**, *22*, 976.

[16] R. Luxenhofer, G. Sahay, A. Schulz, D. Alakhova, T. K. Bronich, R. Jordan, A. V. Kabanov, *J. Controlled Release* **2011**, *153*, 73.

[17] R. Luxenhofer, Y. Han, A. Schulz, J. Tong, Z. He, A. V. Kabanov, R. Jordan, *Macromol. Rapid Commun.* **2012**, *33*, 1613.

[18] L. Tauhardt, K. Kempe, M. Gottschaldt, U. S. Schubert, *Chem. Soc. Rev.* **2013**, *42*, 7998.

[19] J. Ulbricht, R. Jordan, R. Luxenhofer, *Biomaterials* **2014**, *35*, 4848.

[20] Z. He, L. Miao, Y. Jiang, D. Y. Alakhova, R. Jordan, D. Manickam, R. Luxenhofer, A. V. Kabanov, *Macromol. Biosci.* **2015**, *15*, 1004.

[21] Z. He, A. Schulz, X. Wan, J. Seitz, H. Bludau, D. Y. Alakhova, D. B. Darr, C. M. Perou, R. Jordan, I. Ojima, A. V. Kabanov, R. Luxenhofer, *J. Controlled Release* **2015**, *208*, 67.

[22] C. A. Fustin, H. M. L. Thijs-Lambermont, S. Hoeppener, R. Hoogenboom, U. S. Schubert, J. F. Gohy, *J. Polym. Sci., Pol. Chem.* **2010**, *48*, 3095.

[23] U. Mansfeld, S. Hoeppener, K. Kempe, J. M. Schumers, J. F. Gohy, U. S. Schubert, *Soft Matter* **2013**, *9*, 5966.

[24] R. Ivanova, T. Komenda, T. B. Bonné, K. Lüdtke, K. Mortensen, P. K. Pranzas, R. Jordan, C. M. Papadakis, *Macromol. Chem. Phys.* **2008**, *209*, 2248.

[25] J. S. Pedersen, P. Schurtenberger, *Macromolecules* **1996**, *29*, 7602.

[26] W.-R. Chen, P. Butler, L. J. Magid, *Langmuir* **2006**, *22*, 6539.

[27] A. Guinier, F. Fournet, *Small-Angle Scattering of X-rays*, Wiley, New York **1955**.

[28] G. Porod, *Kolloidn. Zh.* **1951**, *123*, 83.

[29] R.-J. Roe, *Methods of X-Ray and Neutron Scattering in Polymer Science*, Oxford University Press, New York **2000**.

[30] P. Bartlett, R. H. Ottewill, *J. Chem. Phys.* **1992**, *96*, 3306.

[31] J. K. Percus, G. J. Yevick, *Phys. Rev.* **1958**, *110*, 1.

[32] K. Larson-Smith, A. Jackson, D. C. Pozzo, *J. Colloid Interface Sci.* **2010**, *343*, 36.

[33] M. Litt, F. Rahl, L. G. Roldan, *J. Polym. Sci., Part A-2: Polym. Phys.* **1969**, *7*, 463.

[34] Chemspider Taxol, www.chemspider.com/Chemical-Structure.10368587.html (accessed: September 2014).

[35] S. R. Kline, *J. Appl. Crystallogr.* **2006**, *39*, 895.

[36] P.-C. Chiang, S. Gould, M. Nannini, A. Qin, Y. Deng, A. Arrazate, K. Kam, Y. Ran, H. Wong, *Nanoscale Res. Lett.* **2014**, *9*, 156.

[37] Y. Seo, A. Schulz, Y. Han, Z. He, H. Bludau, X. Wan, J. Tong, T. K. Bronich, M. Sokolsky, R. Luxenhofer, R. Jordan, A. V. Kabanov, *Pol. Adv. Technol.* **2015**, *26*, 837.